RSC Advances

ROYAL SOCIETY OF CHEMISTRY

www.rsc.org/advances

Journal Name

ARTICLE

Panchromatic Quasi-Monolayer of Ag Nanoparticles for High-Efficiency Dye-Sensitized Solar Cells

Received 00th January 20xx,
Accepted 00th January 20xx

DOI: 10.1039/x0xx00000x

www.rsc.org/

Hyun-Young Kim, and Jung Sang Suh*

We developed a panchromatic quasi-monolayer of Ag nanoparticles (NPs) whose localized surface plasmon resonances take place in all the visible range and applied this technique to fabricate dye-sensitized solar cells (DSSCs). Three kinds of Ag NPs, whose λ_{max} were at 540, 620 and 470 nm, were fabricated. We immobilized them on a photoactive film of TiO_2 NPs coated with poly(4-vinylpyridine) (P4VP), and then coated P4VP again, and then deposited a scattering layer. Most Ag NPs were immobilized individually without aggregation, and formed a quasi-monolayer. By constructing a panchromatic quasi-monolayer between the photoactive and scattering layers, the efficiency was enhanced from 8.9 ± 0.3 % to 11.0 ± 0.4%, mainly by enhancing the photocurrent density. The photocurrent density might be enhanced by enhancement of light absorption and electron transfer yield. Absorption of dye molecules might be enhanced on or near the surface of Ag NPs by the localized surface plasmons. Absorption of dye molecules, particularly molecules not adsorbed on or near the surface, could be enhanced by the scattered light, since the quasi-monolayer of Ag NPs scattered light strongly. Owing to the enhanced dye absorption, we could reduce greatly the thickness of the photoactive layer. The thickness was about 4.5 μm, corresponding to about one-half the optimum length for the DSSCs not included metal NPs. The electron transfer yield to the electrode might be enhanced by being reduced the electron transfer length. Our general method could be used in fabrication of other types of solar cells.

Introduction

Localized surface plasmon resonances (LSPRs) are non-propagating excitations of the conduction electrons of metal nanoparticles (NPs) coupled to the electromagnetic field.[1,2] When the frequency of light photons matches the natural frequency of the collective oscillation of conduction electrons in metal NPs, LSPR is excited. LSPRs create sharp spectral scattering and absorption peaks as well as strong electromagnetic near-field enhancements. The principle of LSPR has been applied to increase the optical absorption and/or photocurrent in a wide range of solar cell configurations.[3-25] However, there is relatively less effort to apply the enhanced light scattering property of metal NPs to improve the energy conversion efficiency of solar cells.

For all the reports of plasmonic DSSCs, the energy conversion efficiency increased up to a certain weight percent of Ag or Au NPs to TiO_2 NPs but then decreased when the weight percent was further increased.[17-26] Recently, Kim *et al.* have proved that this is due to aggregation of metal NPs.[25,26] In the fabrication of photoactive films, metal NPs and TiO_2 NPs were mixed together and then coated on an ITO or FTO glass. Therefore, in principally, aggregations between metal NPs could not be prevented, particularly at a relatively high weight percent of metal NPs. When metal NPs are aggregated, the localized plasmon resonance frequency is red shifted.[27,28] N719 dye, which is the most used dye in DSSCs, has two strong absorption bands centered at 393 and 533 nm. The solar intensity is much stronger at 533 nm than 393 nm, and the band centered at 533 nm could absorb more solar light than that centered at 393 nm. Spherical silver NPs have a LSPR band centered at near 400 nm, while gold NPs at near 520 nm with an increasing strong back ground from 500 nm to UV.[24-25,28] Therefore, to optimize the spectral overlap between the band at 533 nm of N719 dye and the LSPR band of metal NPs, Ag NPs should be aggregated to the dimer or trimer, while Au NPs should be remained individually without aggregation. When Au NPs are aggregated or the cluster size of Ag NPs becomes larger than dimer or trimer, the localized plasmon resonance is shifted to red. In this case, the spectral overlap between the absorption of N719 dye molecules and the LSPR of metal NPs may be reduced, and consequently the plasmon-enhanced absorption of the dye molecules will be reduced.

Ag nanoplates have two localized plasmon resonances, due to the in-plane and out-of-plane resonances, in the visible region. With increasing the size of Ag nanoplates, the wavelength of the in-plane plasmon near 530 nm is red shifted, while that of the out-of-plane plasmon near 400 nm is almost not shifted.[26] By controlling the size and geometry, the LSPR of Ag nanoplates could be turned. Colloid solutions like Ag or Au are very stable because their colloid particles have the same surface charge and repel each other. When Ag or Au NPs are immobilized on the plate coated with poly(4-vinyl pyridine) (P4VP), they are immobilized individually without aggregation due to the repulsion.[28]

Herein, we have fabricated three kinds of Ag NPs whose extinction maximum wavelengths are 540, 620 and 470 nm. By immobilizing them on the film of TiO_2 NPs coated with P4VP

[a] *Nano-materials Laboratory, Department of Chemistry, Seoul National University, Kwanakro 1, Kwanakgu, Seoul 151-742, Republic of Korea.*
E-mail: jssuh@snu.ac.kr, FAX: 82-2-875-6636, Tel: 82-2-880-7763.

†Electronic Supplementary Information (ESI) available: Additional information regarding the dependence of the photovoltaic parameters of the DSSCs included a quasi-monolayer of Ag NPs on the coating time of P4VP, and on the immobilization time of Ag NPs. See DOI: 10.1039/x0xx00000x

without aggregation, we fabricated a panchromatic quasi-monolayer of Ag NPs whose LSPR took place in the entire visible region. DSSCs included a panchromatic quasi-monolayer of Ag NPs between the photoactive layer of TiO_2 NPs and scatting layer were very effective, and the power conversion efficiency was enhanced from 8.9 ± 0.3 % to 11.0 ± 0.4%. The efficiency of 11.4% achieved here is the highest published so far for plasmonic DSSCs and about the highest value for the DSSCs based on N719 dye and TiO_2 NPs.

Experimental

Synthesis of colloidal Ag NPs

Ag NPs were synthesized by a rapid thermal process.[29] 25 mL of 0.1 mM silver nitrate, 1.5 mL of 30 mM trisodium citrate, 1.5 mL of 0.7 mM poly(vinylpyrolidone) (weight average molecular weight ; ~29000 g/mol) and 60 μL of 30 wt% hydrogen peroxide were mixed together. To this solution, 60 μL of X (60, 80, 100) mM sodium borohydride was rapidly injected and then stirred vigorously for 45 min. Colour of colloid solutions became pale yellow after injection, and then slowly changed to orange or purple or blue, indicating the growing of Ag NPs. The size of Ag NPs was controlled by varying the concentration of the sodium borohydride solution injected.

Fabrication of DSSCs

A TiO_2 blocking layer was formed on the surface of fluorine-doped thin oxide (FTO) glass by spin-coating with 5 wt% of titanium di-isopropoxide bis(acetylacetonate) in butanol and annealed at 450 ^{o}C for 1 h. Conventional photoanodes were prepared by depositing TiO_2 NPs paste (T/SP, solaronix) on the surface of the FTO glass using a doctor blade technique, and then heated gradually at 450 ^{o}C for 1 h. The scheme for constructing a quasi-monolayer of Ag NPs between the layer of TiO_2 NPs and scattering layer is shown in Figure 5. The surface of the conventional photoanodes was coated with Poly (4-vinylpyridine) (P4VP) by dipping in a P4VP solution (0.3g of P4VP was dissolved in ethanol 100mL) for 1 h 30 min, and then were washed the surface by ethanol sufficiently, and then dried in air. The photoanode coated with P4VP was put in a Petri dish containing a 15 ml of Ag NPs solution for 12 h to immobilize Ag NPs on it, and then washed the surface by H_2O and Ethanol. After drying, the surface was coated with P4VP again, and then a paste for the scattering layer (DSL 18NR-AO, Dyesol) was coated by doctor blade and then sintered at 450^{o}C for 30 min. The resulting films were treated in titanium isopropoxide (TIP) solutions (0.1 M in isopropyl alcohol) for 30 min at 90 ^{o}C, and followed by annealing at 350 ^{o}C for 10 min. For the films included Ag NPs, additionally hydrogen was flowed at 450 ^{o}C for 10 min. The photoanodes were immersed into a N719 (solaronix) dye solution (50mM in EtOH) under heating to 50 ^{o}C for 12 h. Pt-layered counter-electrodes were prepared by drop-coating H_2PtCl_6 solution (0.5 M in EtOH) onto FTO glass and then sintered at 450 ^{o}C for 30 min. The working electrode was assembled with Pt-coated counter electrode by using a 60 μm -thick surlyn. The composition of the electrolyte was as follows: 0.7 M of 1 butyl -3-methyl imidazolium iodide (BMII), 0.03 M of I_2, 0.1 M of guanidium thiocyanate (GSCN), and 0.5 M of 4 *tert*-butyl pyridine (TBP) in a mixture of acetonitrile and valeronitrile (85: 15 v/v).

Characterization of Ag NPs and DSSCs

The structure and size of Ag NPs were confirmed by an energy-filtering transmittance electron microscope (EF-TEM, Carl Zeiss, LIBRA 120) and a field emission scanning electron microscope (FE-SEM) (JSM-6330F, JEOL Inc.). Current density-voltage (J-V) characteristics of the DSSCs were measured using an electrometer (KEITHLEY 2400) under AM 1.5 illumination (100 mW/cm^2) provided by a solar simulator (1 KW xenon with AM 1.5 filter, PEC-L01, Peccel Technologies). The incident photon-to-current conversion efficiency (IPCE) was measured using McScience (model K3100) with reference to the calibrated diode. A 300 W Xenon lamp was used as light source for generation of a monochromatic beam. The bias light was supplied by a 150 W halogen lamp. The spectra of the electrochemical impedance spectroscopy (EIS) were measured with a potentiostat (Solartron 1287) equipped with a frequency response analyzer (Solartron 1260), with the frequency ranging from 10^{-1} to 10^5 Hz. The applied bias voltage and ac amplitude were set at open circuit voltage (V_{oc}) of the DSSCs and 10 mV, respectively. The impedance measurements were carried out at open-circuit potential under AM 1.5 one-sun light illumination.

Results and discussion

Figure 1 shows the scanning electron microscopy (SEM) images of three kinds of Ag NPs immobilized on the surface of cover glass coated with P4VP and schematic of Ag NPs immobilized on P4VP. Most Ag NPs are isolated. Ag NPs shown in Figure 1a are more like spheres, while more like nanoplates in Figure 1b and c. The TEM images of three kinds of Ag NPs are shown in Figure S1, and one of them is shown in Figure 1b as an insert. Their size is about 15 ± 4, 24 ± 3, and 30 ± 4 nm, respectively. Ag NPs are immobilized on P4VP by an attractive interaction between the lone pair electrons on the nitrogen atom of the pyridine ring and Ag NPs(see Figure 1d).

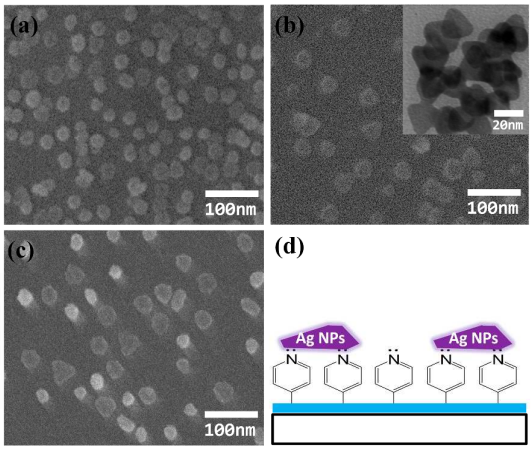

Fig. 1 SEM images of three kinds of Ag NPs immobilized on the surface of cover glass coated with P4VP and schematic of silver NPs immobilized on P4VP. Insert is a TEM image.

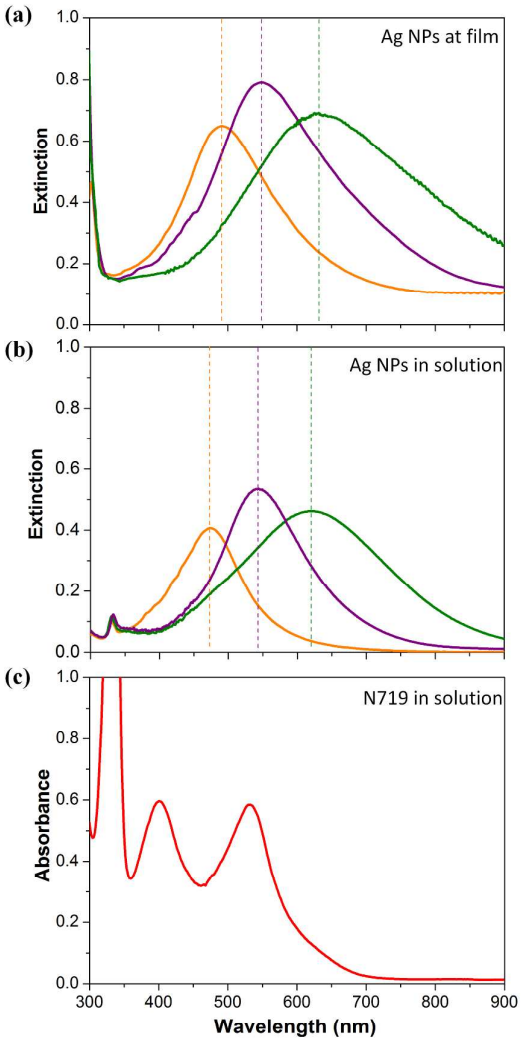

Fig. 2 UV-vis extinction spectra of three kinds of Ag NPs; (a) being immobilized on cover glass coated with P4VP, and (b) their solutions, and (c) UV-vis absorption spectrum of a N719 dye in ethanol solution.

Figure 2 shows the UV-visible extinction spectra of three kinds of Ag NPs immobilized, whose SEM images are shown in Figure 1a-c, and those of their solutions. The extinction maximum of three kinds of Ag NPs immobilized is at 470, 540 and 620 nm, respectively. With increasing the size, the maximum wavelength is shifted to red and the extinction band becomes broad. The spectrum of each kind of Ag NPs immobilized is very similar to that measured in their solution. There is no significant shift in their extinction maximum wavelengths. For Ag nanoplates fabricated by seed-mediated processes have two localized plasmon resonance peaks, due to the in-plane and out-of-plane resonances, near 520 and 400 nm, respectively.[30] The in-plane peak of Figure 2a and b is much broader than that reported, while the out-of-plane peak is relatively much weaker and not distinct well. For a comparison, the absorption spectrum of N719 dye is shown in Figure 2c. There are two visible bands at 398 and 538 nm. The absorption of N719 dye is relatively weak near 450 nm and longer wavelength region than 600 nm.

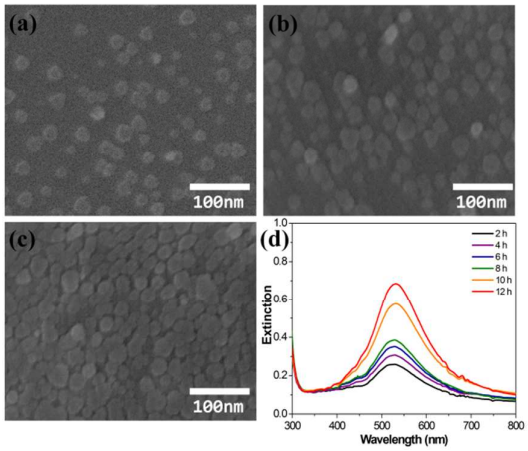

Fig. 3 SEM images of Ag NPs immobilized for 4, 8, and 12 h on the surface of cover glass coated with P4VP, and UV-vis extinction spectra measured by varying the immobilization time. The average size is about 24 ± 3 nm.

Figure 3 shows the SEM images of Ag NPs immobilized for 4, 8, and 12 h and UV-visible extinction spectra measured by varying the immobilization time. Ag NPs are completely isolated when the immobilization time was relatively short. With increasing the immobilization time the surface coverage is increased, and some seem to be aggregated. Although the extinction intensity is increased greatly with increasing the immobilization time, the extinction maximum wavelength is only slightly red shifted. This may mean that aggregation of Ag NPs do not take place greatly in the process of immobilization. Aggregation could be prevented by the repulsion force between Ag NPs having the same surface charge.

Figure 4 shows the SEM images and extinction spectra of three kinds of Ag NPs immobilized on cover glass coated with P4VP in three steps. It should be mentioned that Ag NPs were not distinguished from TiO_2 NPs when they were immobilized on the film of TiO_2 NPs (see Figure S2). When Ag NPs having λ_{max} of 540 nm in the solution phase were immobilized for 4 h, the extinction maximum wavelength was near 540 nm, which was almost the same as that of the Ag NPs in a solution phase (see the black colored spectrum of Figure 4d). The surface coverage of Ag NPs was greater than 50%. When two kinds of Ag NPs having λ_{max} of 540 and 620 nm were immobilized, in sequence, for 4 h each, the λ_{max} was near 575 nm, and a shoulder on the low energy side was significantly increased (see the blue spectrum). When three kinds of Ag NPs having λ_{max} of 540, 620, and 470 nm were immobilized in sequence for 4 h each, the λ_{max} was near 550 nm, and the shoulders on the high and low energy sides were significantly increased compared to the black spectrum (see the red spectrum). The extinction intensity was increased with increasing the total immobilization time.

A conventional photoanode based on TiO_2 NPs is fabricated by formation of a blocking layer on FTO glass, and then depositing a

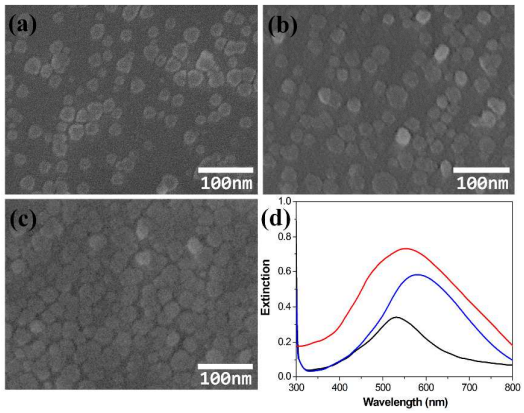

Fig. 4 The SEM images (a-c) and extinction spectra (d) of Ag NPs immobilized on cover glass coated with P4VP: (a and black spectrum in (d)) Ag NPs having λ_{max} of 540 nm in the solution phase were immobilized for 4 h, (b and blue one) two kinds of Ag NPs having λ_{max} of 540 and 620 nm were immobilized, in sequence, for 4 h each, and (c and red one) three kinds of Ag NPs having λ_{max} of 540, 620, and 470 nm were immobilized, in sequence, for 4 h each.

relatively thick layer of TiO_2 NPs, and then depositing scattering layer. We have included a quasi-monolayer of Ag NPs between the layer of TiO_2 NPs and the scattering layer. The schematics of the fabrication processes are shown in Figure 5. P4VP was coated on the surface of the film of TiO_2 NPs deposited on the FTO glass, which had formed a blocking layer on its surface, and then Ag NPs were immobilized on the surface of P4VP by placing the FTO glass coated with P4VP in Ag colloid solutions. After immobilizing, P4VP was coated again to prevent moving of Ag NPs, and then, scattering layer was deposited by a doctor blade printing, and then sintered. For a panchromatic quasi-monolayer of Ag NPs whose extinction takes place in a whole visible region, three kinds of Ag NPs, whose maximum absorptions were at 540, 620 and 470 nm, were immobilized in sequence. In the immobilization of Ag NPs, the surface coverage was increased with increasing the immobilization time but not linearly. The increasing rate of the coverage was decreased with increasing immobilization time. Due to this non-linearity, it was very hard to optimize a quasi-monolayer consisting of three kinds of Ag NPs. To simplify, we immobilized each kind of Ag NPs for an equal time. In this case, the efficiency was critically affected by the immobilization order of three kinds of Ag NPs. The efficiency was highest when Ag NPs of 540 nm in λ_{max} was immobilized first, and then 620 nm, and finally 470 nm (see Table S7). This could be related to the fact that among the films prepared by varying immobilization order of three kinds of Ag NPs, the film prepared by immobilizing Ag NPs having λ_{max} of 540 nm first, and then 620 nm, and then 470 nm showed the broadest extinction spectrum, and had the highest overlap with the spectrum of N719 dye (see Figure S3). The efficiency of the DSSCs included a quasi-monolayer consisting of three kinds of Ag NPs was highest when the immobilization time of each type of Ag NPs was 4 h (12 h in total) (see Table S6). Also, the efficiency was slightly affected by the coating times of P4VP before and after immobilization of Ag NPs (see Tables S1-5). It was highest when the coating time of P4VP

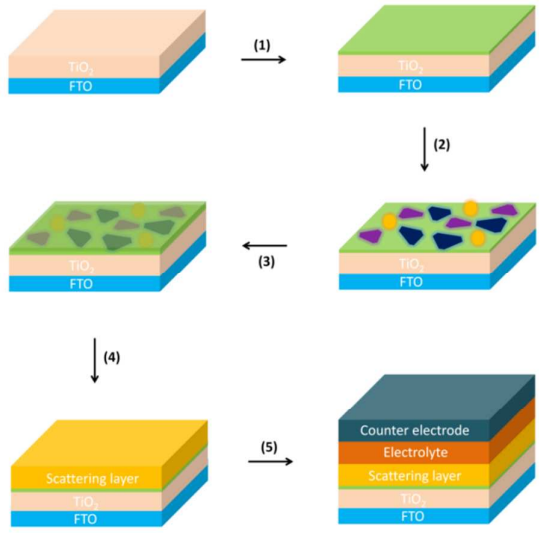

Fig. 5 Scheme for construction of the DSSC included a quasi-monolayer of Ag NPs between the layer of TiO_2 NPs and scattering layer: (i) coating P4VP, (ii) immobilization of Ag NPs, (iii) coating P4VP again, (iv) depositing a scattering layer, and fabrication of a DSSC.

before and after immobilization of Ag NPs was 1.5 and 1 h, respectively.

To prevent corrosion of Ag NPs, TIP was treated. TIP treatment is known to be an efficient method to prevent silver corrosion and electron leaking from Ag NPs. Jeong et al. have studied the effect of treating Ag NPs with TIP in detail and proved that TIP treatment sufficiently can prevent silver corrosion and electron leaking from Metal NPs.[12] The thickness of the photoactive TiO_2 film itself was about 4.5 μm in the DSSCs included a quasi-monolayer of Ag NPs, while 9 μm in the conventional DSSCs. With including the scattering layer, the thickness of the photoactive TiO_2 film was about 13 μm for the DSSCs included a quasi-monolayer of Ag NPs, while 17 μm for the conventional DSSCs.

It should be mentioned that the morphology of Ag nanoplates could be modified by sintering at 450 ^{o}C. When Ag nanoplates are sintered at a relatively high temperature, they will be changed ultimately to spherical silver to minimize their surface area. It is known that the LSPR band of spherical Ag NPs centers at near 400 nm.[28] Therefore, a blue shift of the LSPR band of our Ag nanoplates could take place when the morphology was modified by sintering. However, Ag nanoplates included in our DSSCs existed between the photoactive and scattering layers. This means that Ag nanoplates were surrounded by a large amount of TiO_2 NPs. Also, the surface of Ag nanoplates was coated with TiO_2 to prevent corrosion. Therefore, the morphology change of Ag nanoplates by sintering could be reduced greatly under our conditions. We tried to observe the blue shift of Ag nanoplates surrounded by TiO_2 NPs by sintering. However, we could not observe the LSPR band of Ag nanoplates itself due to a strong background of TiO_2.

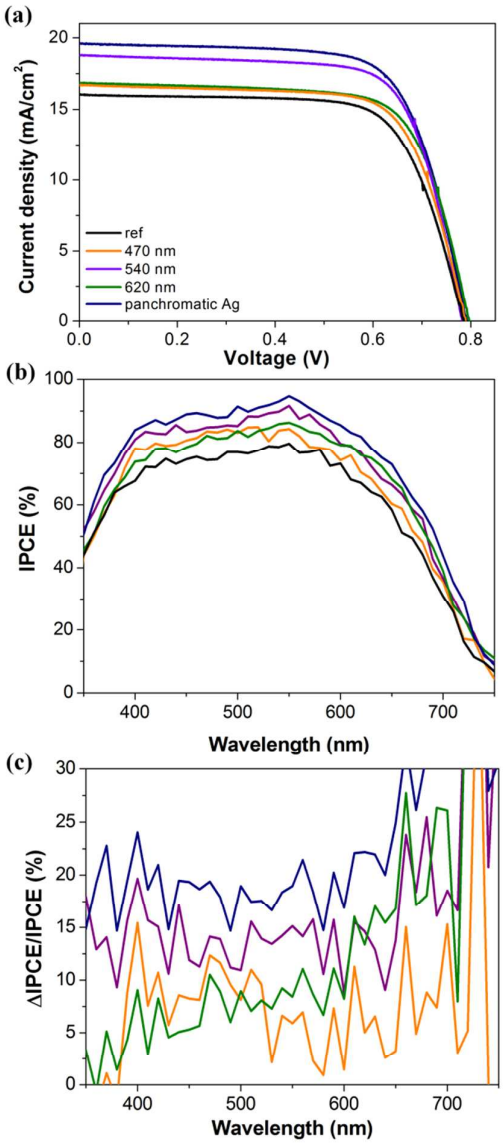

Fig. 6 (a) Photocurrent density-voltage (*J-V*) curves and (b) IPCE spectra measured from the DSSCs based on films of TiO_2 NPs, with and without being constructed a quasi-monolayer of Ag NPs between the layer of TiO_2 NPs and the scattering layer, and (c) the relative IPCE improvement factor [ΔIPCE (λ) / IPCE (λ) %] spectra. The legend represents the values of the λ_{max} of in-plane dipolar plasmon resonance peak of the Ag NPs included in the fabrication of the DSSCs.

In Figure 6a, the photocurrent density-voltage (*J-V*) curves measured in air mass 1.5 sunlight from the DSSCs based on films of TiO_2 NPs, with and without being constructed a quasi-monolayer of Ag NPs between the layer of TiO_2 NPs and the scattering layer, are compared. The photovoltaic parameters are summarized in Table 1. The total immobilization time of single kind or three kinds of Ag NPs was the same as 12 h. For a panchromatic quasi-monolayer, Ag NPs with λ_{max} at 540 nm was immobilized first, and then those at 620 nm, and then those at 470 nm. For the DSSC not included a monolayer of Ag NPs, the short-circuit current density (J_{sc}), open-circuit voltage (V_{oc}), fill factor (*ff*), and overall conversion efficiency (η) were 16.23 ± 0.42 mA/cm^2, 0.80 ± 0.02 V, 0.69 ± 0.01, and 8.9 ± 0.3%, respectively. Among the DSSCs included single-type Ag NPs as a quasi-monolayer, one included Ag NPs whose λ_{max} was 540 nm shows the highest efficiency. The photovoltaic parameters were 18.11 ± 0.55 mA/cm^2, 0.79 ± 0.01 V, 0.70 ± 0.02, and 10.5 ± 0.3%, respectively. For the DSSC included a quasi-monolayer consisting of three kinds of Ag NPs, the photovoltaic parameters were 19.27 ± 0.53 mA/cm^2, 0.79 ± 0.03 V, 0.71 ± 0.03, and 11.0 ± 0.4%, respectively. It is concluded that the DSSCs included a quasi-monolayer of three kinds of Ag NPs are more effective for light harvesting than the DSSCs included that of single kind of Ag NPs or conventional DSSCs. The open-circuit voltages and fill factor are not changed significantly. The efficiency enhancement by inclusion a quasi-monolayer of Ag NPs is mainly caused by the increase in photocurrent density. The efficiency of 11.4% achieved here is the highest published so far for plasmonic DSSCs.[24,31]

Table 1. Photovoltaic parameters measured from the DSSCs based on films of TiO_2 NPs, with and without being constructed a quasi-monolayer of Ag NPs between the layer of TiO_2 NPs and the scattering layer.

	V_{oc} (V)	J_{sc} (mA/cm^2)	*ff* (%)	η (%)
470 nm	16.23 ± 0.42	0.80 ± 0.02	0.69 ± 0.01	9.3 ± 0.2
540 nm	18.11 ± 0.55	0.79 ± 0.01	0.70 ± 0.02	10.5 ± 0.3
620 nm	16.98 ± 0.48	0.78 ± 0.01	0.71 ± 0.02	9.7 ± 0.2
panchromatic	19.27 ± 0.53	0.79 ± 0.03	0.71 ± 0.03	11.0 ± 0.4
reference	16.20 ± 0.41	0.78 ± 0.02	0.70 ± 0.03	8.9 ± 0.3

The incident photon-to-current conversion efficiency (IPCE) spectra measured from the five DSSCs are shown in Figure 6b. By construction of a quasi-monolayer of Ag NPs between the layer of TiO_2 NPs and the scattering layer, IPCE over the wavelength range 400 to 700 nm is enhanced, exhibiting the maximum wavelength of near 550 nm which is closely associated with N719 dye absorption. The DSSC included a quasi-monolayer of three kinds of Ag NPs shows highest intensity over the whole range of wavelengths (400 - 700 nm). The relative intensity of IPCE spectra of the DSSCs included a quasi-monolayer of Ag NPs is closely related to the degree of the spectral overlap between the extinction bands of Ag NPs included in fabrication of DSSCs and the absorption bands of N719 dye. It is clearly seen in the IPCE improvement factor spectra shown in Figure 6c. The factor has been calculated by the following equation: ΔIPCE (λ) / IPCE (λ) % = [($IPCE_{DSSC\ included\ a\ Ag\ NPs'\ layer\ (\lambda)}$ - $IPCE_{DSSC\ not\ included\ a\ Ag\ NPs'\ layer\ (\lambda)}$) / $IPCE_{DSSC\ not\ included\ a\ Ag\ NPs'\ layer\ (\lambda)}$] x 100. In the IPCE improvement factor spectra, the intensity of the DSSC included a quasi-monolayer of Ag NPs whose λ_{max} is 620 nm is stronger in the low energy region but weaker in high energy region than that of the DSSC included a quasi-monolayer of Ag NPs whose λ_{max} is 470 nm.

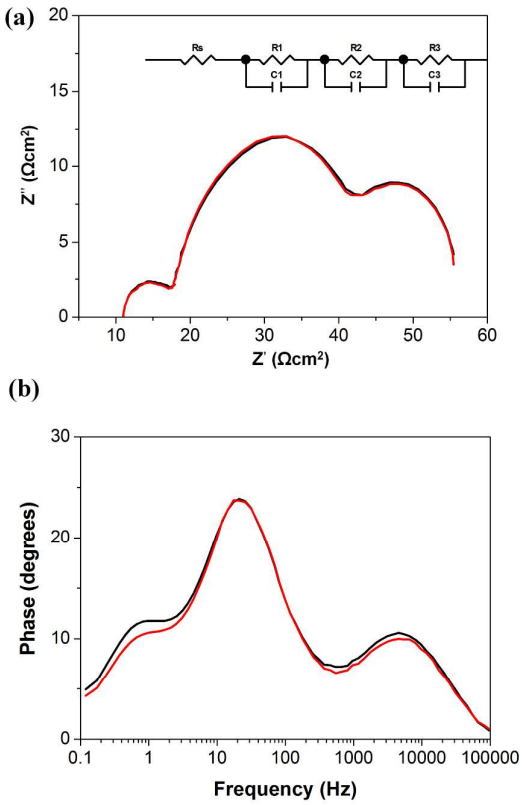

Fig. 7 Electrochemical impedance spectra of the DSSCs based on the photoactive film of TiO_2 NPs with (red) and without (black) including a panchromatic quasi-monolayer of Ag NPs between the layer of TiO_2 NPs and the scattering layer; (a) Nyquist plot and (b) Bode plot. The thickness of both photoactive films of TiO_2 NPs was the same as 4.5 μm.

Figure 7 shows the characteristic electrochemical impedance spectra (EIS) for the DSSCs based on TiO_2 film and TiO_2/Ag nanoplate film. They were recorded in the frequency range of 0.1 Hz to 100 KHz. Each spectrum contains well-defined three semicircles. The hemisphere in the high-frequency region is assign to the parallel combination of the resistance and capacitance at the Pt-FTO/electrolyte and to the interface between FTO and TiO_2 layers, while those in the intermediate and low-frequency regions offer information on the resistance and capacitance at the TiO_2/electrolyte interface and the Nernst diffusion of the electrolyte, respectively.[32] On the Nyquist plot two spectra are almost the same, while on the Bode plot two spectra show a little difference at low and high frequency region. In both spectra, the position of the middle frequency (f_{mid}) peak was the same as 21.23 Hz. The value of the middle frequency (f_{mid}) is related to the inverse of the electron lifetime (τ) as follows: $\tau_{eff} = 1/(2\pi f_{mid})$.[33,34] The calculated electron lifetime was 7.49 ms for the DSSCs based on the photoactive film of TiO_2 NPs with and without including a panchromatic quasi-monolayer of Ag NPs between the layer of TiO_2 NPs and the scattering layer, respectively. Also, the electron lifetime is related to the effective carrier diffusion length (L_n) as follows: $L_n^2 = D_{eff} \times \tau$, where D_{eff} is the effective electron diffusion coefficient and τ is the electron lifetime. Based on the Bisquert model,[35] D_{eff} is described as $D_{eff} = (R_k/R_w)L^2k_{eff}$.[33,34] Where R_w, R_k, L, and k_{eff} represent the resistance of electron transport in the photoanode, the resistance of charge transfer related to recombination, the thickness of the photoanode, and the constant of effective rate for recombination, respectively. The values of these parameters can be obtained from the semicircle of middle frequency in Nyquist and Bode plots. R_w is estimated from diameter of the middle semicircle in the Nyquist plot shown in Figure 7 a, and R_k is determined from the diameter of the middle semicircle in the Nyquist plot obtained under dark conditions (Figure S4). k_{eff} is obtained from the maximum peak frequency obtained from the Bode plot in Figure 7b.[34] The calculated values are summarized in Table S8. The calculated value of L_n for the DSSCs based on the photoactive film of TiO_2 NPs with and without including a panchromatic quasi-monolayer of Ag NPs was 7.10 and 7.98 μm, respectively. The results indicate that there is no significant difference both in the electron lifetime and effective carrier diffusion length. This could be due to the fact that the panchromatic layer of Ag NPs was constructed on the surface of the photoactive layer, and it was not on the path of electron transfer. Therefore, basically the electron lifetime and effective carrier diffusion length could not be affected by the panchromatic layer.

By construction of a panchromatic quasi-monolayer of Ag NPs between the photoactive and scattering layers and reducing the thickness of the photoactive layer, the power conversion efficiency has been enhanced up to 11.4%, mainly by enhancing the photocurrent density. The efficiency of 11.4% achieved here is the highest published so far for plasmonic DSSCs.[24] The photocurrent density might be enhanced by enhancement of light absorption and electron transfer yield to the electrode. An enhanced light absorption of dye molecules could take place on or near surface of metal NPs by LSPRs. The LSPRs decay either radiatively or into (quasi) particles such as electron-hole (e-h) pairs.[36] The former decay path gives rise to the dramatic electromagnetic field enhancements, for instance, as in surface-enhanced Raman spectroscopy. By the latter decay path, the light absorption of dye molecules adsorbed on or near Ag NPs is enhanced.[37] Absorption of dye molecules, particularly molecules not adsorbed on or near the surface of Ag NPs, could be enhanced by the scattered light, since the quasi-monolayer of Ag NPs scattered light strongly. Besides these two enhanced absorptions caused by Ag NPs, the normal absorption of the incident light by the dye molecules adsorbed on the surface of TiO_2 NPs takes place. This normal absorption may increase with increasing the number of dye molecules up to a certain value, since the number of photons of solar light is limited. Therefore, this absorption will increase with increasing the thickness of the photoactive layer consisting of TiO_2 NPs where dye molecules are adsorbed. The plasmon enhanced absorption takes place only to the molecules adsorbed on or near the surface of Ag NPs, and it is not affected directly by the thickness of the photoactive layer. However, it is affected by the light intensity reached to the quasi-monolayer. Therefore, the plasmon enhanced absorption may be critically affected by the location of quasi-

monolayer of Ag NPs, since the intensity of light reached to the quasi-monolayer is decreased with increasing the thickness of the photoactive layer. With increasing thickness of the photoactive layer, absorption of the scattered light could be affected by two opposite factors. With increasing the thickness of the photoactive layer, the intensity of light reached to the quasi-monolayer is decreased, and that of the scatter light is also decreased. However, the number of dye molecules, which could absorb the scattered light, is increased with increasing the thickness of the photoactive layer. Consequently, the dye absorption could be affected by the thickness of the photoactive layer existing in front of a panchromatic quasi-monolayer. Actually, the efficiency of the DDSCs constructed a panchromatic quasi-monolayer between the photoactive and scattering layers was affected by the thickness of the photoactive layer. When the thickness of the photoactive layer was 3.0, 4.5, and 9.0 μm, the efficiency was 9.99, 11.4, and 10.7%, respectively. A more precise optimization of the thickness should be studied in detail. At least, a high efficiency was achieved by construction of a panchromatic quasi-monolayer of Ag NPs on the surface of photoactive layer whose thickness was 4.5 μm. This thickness is much thinner than the optimum length (about 9 μm) for the DSSCs based only TiO_2 NPs.[38] There is no doubt that the electron transfer yield to the electrode increases with decreasing the transfer length. Therefore, the high efficiency might be contributed partially by the reduced thickness of the photoactive film.

It is not a difficult process to construct a quasi-monolayer of Ag NPs between the layer of TiO_2 NPs and the scattering layer. The optical property of the quasi-monolayer of Ag NPs is not affected critically by the fabrication technique, since most Ag NPs are immobilized without aggregation due to repulsion between Ag NPs. Also, the panchromatic property is made quite uniformly on the whole area of a quasi-monolayer, since Ag NPs are immobilized randomly. This general method to construct a quasi-monolayer of Ag NPs could be used in fabrication of other types of solar cells.

Conclusions

We have developed a quasi-monolayer of Ag NPs, without making aggregation, whose extinction takes place in all the visible range and applied this technique to construct dye-sensitized solar cells (DSSCs). Three kinds of Ag NPs, whose λ_{max} were at 540, 620 and 470 nm, were immobilized, in sequence, on a photoactive film of TiO_2 NPs coated with P4VP, and then coated P4VP again, and then deposited a scattering layer. The efficiency of the DSSCs included a quasi-monolayer of Ag NPs between the layer of TiO_2 NPs and the scattering layer was enhanced up to 11.4%. The efficiency of 11.4% achieved here is the highest published so far for plasmonic DSSCs. A high efficiency is contributed by the increased light absorption and reduced electron transfer length. Our general and simple method could be used in fabrication of other types of solar cells.

Acknowledgements

This work was supported by Basic Study program through the National Research Foundation of Korea funded by the Ministry of Education, Science and Technology (2012R1A1A2003515), the New & Renewable Energy of the Korea Institute of Energy Technology Evaluation and Planning (KETEP) grant (305-20110024) funded by the Ministry of Knowledge Economy, Republic of Korea, and the BK21 program.

Notes and references

Nano-materials Laboratory, Department of Chemistry, Seoul National University, Kwanakro 1, Kwanakgu, Seoul 151-742, Republic of Korea.

*To whom correspondence should be addressed.

E-mail: jssuh@snu.ac.kr, FAX: 82-2-875-6636, Tel: 82-2-880-7763.

1. M. E. Stewart, C. R. Anderton, L. B. Thompson, J. Maria, S. K. Gray, J. A. Rogers, and R. G. Nuzzo, *Chem. Rev.* 2008, **108**, 494-521.
2. N. Zhou, V. L´opez-Puente, Q. Wang, L. Polavarapu, I. Pastoriza-Santos, and Q.-H. Xu, *RSC Adv.* 2015, **5**, 29076
3. M. Ihara, K. Tanaka, K. Sakaki, I. Honma, and K. Yamada, *J. Phys. Chem. B.* 1997, **101**, 5153–5157.
4. S. D. Standridge, G. C. Schatz, and J. T. Hupp, *Langmuir,* 2009, **25**, 2596–2600.
5. A. Baba, K. Wakatsuki, K. Shinbo, K. Kato, and F. Kaneko, *J. Mater. Chem.* 2011, **21**, 16436–16441.
6. Y. Wang, J. Zhai, and Y. Song, *Phys. Chem. Chem. Phys.* 2015, **17**, 5051
7. Y. Wang, J. Zhai, and Y. Song, *RSC Adv*. 2015, **5**, 210
8. J. -L. Wu, F. -C. Chen, Y. -S. Hsiao, F. –C. Chien, P. Chen, C. –H. Kuo, M. H. Huang, and C. -S. Hsu, *ACS Nano*, 2011, **5**, 959–967.
9. W. Jiang, H. Liu, L. Yin, and Y. Yin, *J. Mater. Chem. A*, 2013, **1**, 6433–6440.
10. S. D. Standridge, G. C. Schatz, and J. T. Hupp, *J. Am. Chem. Soc.* 2009, **131**, 8407–8409
11. M. D. Brown, T. Suteewong, R. S. S. Kumar, V. D'Innocenzo, A. Petrozza, M. M. Lee, U. Wiesner, and H. J. Snaith, *Nano Lett.* 2011, **11**, 438–445.
12. N. C. Jeong, C. Prasittichai, J. T. Hupp, *Langmuir*, 2011, **27**, 14609-14614.
13. Y. –C. Yen, P. –H. Chen, J. –Z. Chen, J. –A. Chen, and K. –J. Lin, *ACS Appl. Mater. Interfaces*, 2015, **7**, 1892-1898.
14. T. Kawawaki, Y. Takahashi, and T. Tatsuma, *J. Phys. Chem. C*, 2013, **117**, 5901-5907.
15. S. W. Sheehan, H. Noh, G. W. Brudvig, H. Cao, and C. A. Schmuttenmaer, *J. Phys. Chem. C*, 2013, **117**, 927-934.
16. J. T. Park, W. S. Chi, H. Jeon, and J. H. Kim, *Nanoscale*, 2014, **6**, 2718
17. J. Yun, S. H. Hwang, and J. Jang, *ACS Appl. Mater. Interfaces*, 2015, **7**, 2055-2063.

18. Y. H. Jang, Y. J. Jang, S. T. Kochuveedu, M. Byun, Z. Lin, and D. H. Kim, *Nanoscale*, 2014, **6**, 1823
19. M. K. Gangishetty, R. W. J. Scott, and T. L. Kelly, *Langmuir*, 2014, **30**, 14352-14359.
20. H. Jung, B. Koo, J. –Y. Kim, T. Kim, H. J. Son, B. S. Kim, J. Y. Kim, D. –K. Lee, H. Kim, J. Cho, and M. J. Ko, *ACS Appl. Mater. Interfaces*, 2014, **6**, 19191-19200.
21. H. F. Zarick, O. Hurd, J. A. Webb, C. Hungerford, W. R. Erwin, and R. Bardhan, *ACS Photonics*, 2014, **1**, 806-811.
22. M. K. Gangishetty, K. E. Lee, R. W. J. Scott, and T. L. Kelly, *ACS Appl. Mater. Interfaces*, 2013, **5**, 11044-11051.
23. H. Choi, W. T. Chen, P. V. Kamat, *ACS Nano,* 2012, **6**, 4418.
24. X. Dang, J. Qi, M. T. Klug, P. -Y. Chen, D. S. Yun, N. X. Fang, P. T. Hammond, and A. M. Belcher, *Nano Lett.* 2013, **13**, 637–642
25. H. -Y. Kim, D. H. Song, H. Yoon, and J. S. Suh, *RSC Adv.*, 2015, **5**, 27464
26. H. -Y. Kim, W. -Y. Rho, H. Y. Lee, Y. S. Park, J. S. Suh, *Solar Energy* 2014, **109**, 61.
27. M. Rycenga, M. R. Langille, M. L. Personick, T. Ozel, C. A. Mirkin, *Nano Lett.* 2012, **12**, 6218–6222.
28. S. Lee, G. H. Gu, J. S. Suh, *Chem. Phys. Lett.* 2011, **511**, 121.
29. G. M. Metraux, and C. A. Mirkin, *Adv. Mater*. 2005, **17**, 412-415.
30. S. T. Gentry, M. W. J. Bezpalko, *J. Phys. Chem. C*, 2010, **114**, 6989–6993.
31. S. Mathew, A. Yella, P. Gao, R. Humphry-Baker, B. F. E. Curchod, N. Ashari-Astani, I. Tavernelli, U. Rothlisberger, M. K. Nazeeruddin, and M. Gra¨tzel, *Nature Chemistry*, 2014, **6**, 242–247.
32. Y. J. Kim, M. H. Lee, H. J. Kim, G. Lim, Y. S. Choi, N. -G. Park, Kim, K. and W. I. Lee, *Adv. Mater.* 2009, **21**, 3668–3673.
33. J. Song, Z. Yin, Z. Yang, P. Amaladass, S. Wu, J. Ye, Y. Zhao, W.-Q. Deng, H. Zhang, X.-W. Liu, *Chem. Eur. J.* 2011, **17**, 10832 – 10837.
34. Y. Wang, J. Zhai, Y. Song, *RSC Adv.*, 2015, **5**, 210-214.
35. J. Bisquert *J. Phys. Chem. B* 2002, **106**, 325-333.
36. U. Kreibig and M. Vollmer, *Optical Properties of Metal Clusters*, Springer Series in Materials Science, Springer, NY, USA, 1995.
37. C. Langhammer, B. Kasemo1, and I. Zorić, *J. Chem. Phys.* 2007, **126**, 194702-1-11.
38. A. Hagfeldt, G. Boschloo, L. Sun, L. Kloo, and H. Pettersson, *Chem. Rev.* 2010, **110**, 6595–6663.

